Plasmonic rainbow rings induced by white radial polarization

Tzu-Hsiang Lan,[1] Yi-Kuan Chung,[1] Jie-En Li,[2] and Chung-Hao Tien[2,*]

[1]*Department of Photonics and Institute of Electro-optical Engineering, National Chiao Tung University, Hsinchu 30010, Taiwan*

[2]*Department of Photonics and Display Institute, National Chiao Tung University, Hsinchu 30010, Taiwan*

**Corresponding author: chtien@mail.nctu.edu.tw*

Received August 4, 2011; revised January 18, 2012; accepted February 3, 2012;
posted February 9, 2012 (Doc. ID 152389); published March 26, 2012

This Letter presents a scheme to embed both angular/spectral surface plasmon resonance (SPR) in a unique far-field rainbow feature by tightly focusing (effective NA = 1.45) a polychromatic radially polarized beam on an Au (20 nm)/SiO_2 (500 nm)/Au (20 nm) sandwich structure. Without the need for angular or spectral scanning, the virtual spectral probe snapshots a wide operation range (n = 1–1.42; λ = 400–700 nm) of SPR excitation in a locally nanosized region. Combined with the high-speed spectral analysis, a proof-of-concept scenario was given by monitoring the NaCl liquid concentration change in real time. The proposed scheme will certainly has a promising impact on the development of objective-based SPR sensor and biometric studies due to its rapidity and versatility.

OCIS codes: 050.1960, 240.6680, 260.5430.

Surface plasmon resonance (SPR) sensors have been widely used to analyze the optical characteristics of material due to their highly axial resolution and angular/spectral sensitivity via strong confinement of surface plasmon polaritons (SPPs) at the metal-dielectric interface [1]. As an in-plane wave vector of an incident wave matches the resonant condition at the metal–dielectric boundary, a group of free electrons of noble metal is excited to collectively oscillate and propagate as the surface wave [2]. The mechanism of SPPs excitation was generally induced by a prism coupler, first proposed by Kretschmann and Raether [3] and Otto [4] in the 1960s . Kano and Knoll then replaced the prism by a collinear object to enable a universal wave vector without the need for angular scanning. As a result, the presence of SPR was observed by a dark resonance ring at the far-field pupil plane [5]. Based on the collinear setup, many researchers introduced a radially polarized beam as the virtual Bessel probe to improve the conversion efficiency of SPPs and spatial resolution [6]. Impressive two-dimensional refractive index images of a cell with fine details and high contrast were obtained and remained constrained with a monochromatic illumination [7,8]. The necessity of relying on spectral/angular scanning has prevented to a large extent a widespread diffusion of the SPR sensor, thus precluding its transfer to clinical practice. A drive for scanning-free operation prompted us to develop a white light radial polarization that excites the SPPs at the entire spectral/angular domain and that ultimately implements a snapshot of two-dimensional SPR information.

Figure 1 schematically illustrates a white radial polarization enabling SPR (WRP-SPR) sensor, based on an inverted microscopy (Olympus IX81). A white light source manufactured by Luxeon Star (LXHL-NEW8) was used to offer a collimated polychromatic beam. After passing through the polychromatic radially polarized converter (PRPC), a white radial polarized beam was tightly focused by an objective (Olympus PlanApo-N 60x/1.45 oil). The axially symmetric polarization of radial polarization would lead to the entire beam being TM polarized with respect to the metal interface. SPPs were simultaneously excited on the metal in all directions and formed a localized Bessel beam.

A new optical element, based on the dichroic polarizer in segmental arrangement, was proposed to convert the incident white light into radial polarization without dependence of wavelength. As shown in the inset of Fig. 1(a), the PRPC was composed of eight sectors of dichroic polarizer, and each transmission axis was oriented along the radial direction [9]. Unlike other attempts at making phase retardation with specific wavelengths or subject to interferometric accuracy in alignment [10,11], the PRPC was customized by a commercial off-the-shelf polarizer, which significantly reduced the cost compared with other systems and allowed for robust operation [12]. Figures 1(b)–1(d) show the field distribution after passing through the PRPC. As we rotated another linear polarizer to examine the beam quality, the high visibility of the oval dark patterns confirmed that the output polychromatic beam was radially polarized over a large part of the visible frequency. Without loss of generality, any spatially

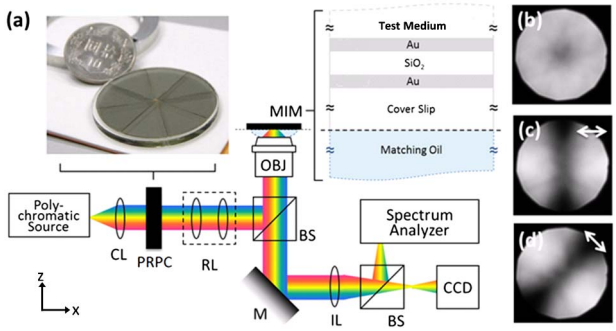

Fig. 1. (Color online) (a) Schematic diagram of the WRP-SPR sensor platform. CL, collimated lens; PRPC, polychromatic radially polarized converter; RL, relay lens; BS, beam splitter; IL, image lens; MIM, Au (20 nm)/SiO_2 (500 nm)/Au (20 nm) sandwich structure. The insets show the experimental intensity distribution of radially polarized beam (b) before and (c), (d) after passing through an analyzer whose transmission axes are indicated by white arrows.

inhomogeneous beam can be obtained by the corresponding polarizer arrangement in a similar approach [13,14].

For a typical Au monolayer in an objective-based SPR sensor, the operation range about the refractive index is mainly limited by the marginal angle of the objective lens [15]. Taking oil immersion lens with NA = 1.45 ($\theta_{\mathrm{Max}} \sim 75.16°$) as an example; the maximum refractive index available is merely 1.28, which is much less than those of common living cells comparable to water (1.33) in the visible spectrum [2,7,15]. In order to extend the operation window, we developed a metal/insulator/metal (MIM) sandwich structure as the SPR coupler. Here we kept the symmetry of the MIM structure and set the overall thickness of Au thin film as 40 nm. SPPs would be excited at the last interface (Au/medium) by the total internal reflection (TIR)—mediated evanescent wave [16].

Compared with the Au monolayer coupler where the SPR is directly induced by the in-plane wave vector of the incident beam, the insulator layer within mid the sandwich structure plays a role into supporting a cavity resonance (CR) mode. Also, an additional SPR mode would be raised by the CR mode—induced evanescent wave coupling. The refractive index and the thickness of the insulator layer have significantly influence on the energy coupling efficiency. To optimize the angular range of the TIR and sustain the wave vector, we chose SiO_2 as the insulator whose refractive index is the same as that of the substrate ($n_{\mathrm{SiO_2}} = n_{\mathrm{Sub}} = 1.5$).

Meanwhile, we modulated the thickness of SiO_2 to observe the sensitivity of the SPR sensor. As the thickness of the SiO_2 layer was zero, the MIM structure was degenerated to the Kretschmann configuration, which reveals relatively noticeable reflectance over the whole incident angle except one dip slightly larger than the critical angle $\theta_{\mathrm{TIR}} \sim 41.87°$. As we increased the thickness of the SiO_2 layer, reflectance at small incident angles was driven by the interference between the multiple reflections within a Fabry-Perot—like resonator where the reflectance was modulated periodically with respect to the insulator thickness. With the same incident angle, the resonance would occur as the insulator thickness is the integer multiple of half a wavelength. Among the large incident angle whose wavevector satisfies the phase matching condition, the cavity resonance modes are likely to be coupled into a new SPR. Because of the presence of a SiO_2 layer with sufficient thickness (>150 nm), the coupled SPR mode would exist subject to smaller propagation constants; thus, test samples with a higher refractive index can be detected effectively at the same objective lens. The coupled SPR mode obviously shows the angular shift and linear dependence in sensitivity. The interested reader can refer to [16] for more details.

The validation of the aforementioned discussion was observed by Fig. 2(a). When a medium was applied, such as water ($n_{\mathrm{water}} = 1.33$), the reflectance dip would exceed the border of the pupil; thus, no SPR was generated at a short wavelength by the monolayer Au SPR sensor. For the MIM structure, on the other hand, the coupled SPR mode induced a sharp resonance dip and covered the visible spectrum, as shown in Fig. 2(b). The corresponding dark ring can be experimentally observed at the exit pupil, where three selective wavelengths across the visible spectrum ($\lambda = 610$, 530, and 450 nm) exhibit

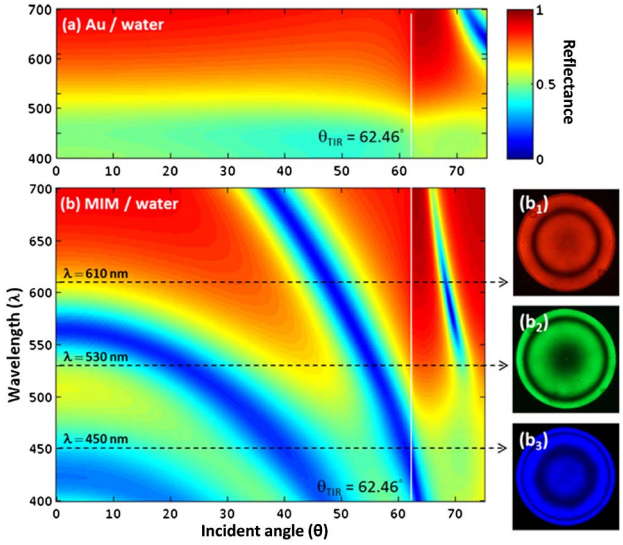

Fig. 2. (Color online) The spectral reflectance with different incident angles when the SPR coupler is (a) a 40 nm Au monolayer and (b) a Au (20 nm)/SiO_2 (500 nm)/Au (20 nm) structure, where the experimental observation [(b1)–(b3)] of dark rings corresponds to resonance at wavelengths of 610, 530, and 450 nm, respectively.

the individual resonance conditions. The experimental results were in close agreement with the simulation and prior literatures with monochromatic illumination (Fig. 3 of [7]).

By tightly focusing a polychromatic radially polarized beam on the Au (20 nm)/SiO_2 (500 nm)/Au (20 nm) sandwich structure, we have the capability to snapshot the existence of SPR in angular/spectral domain via a unique far-field plasmonic rainbow rings, as shown in Fig. 3. A two-dimensional SPR excitation condition can be

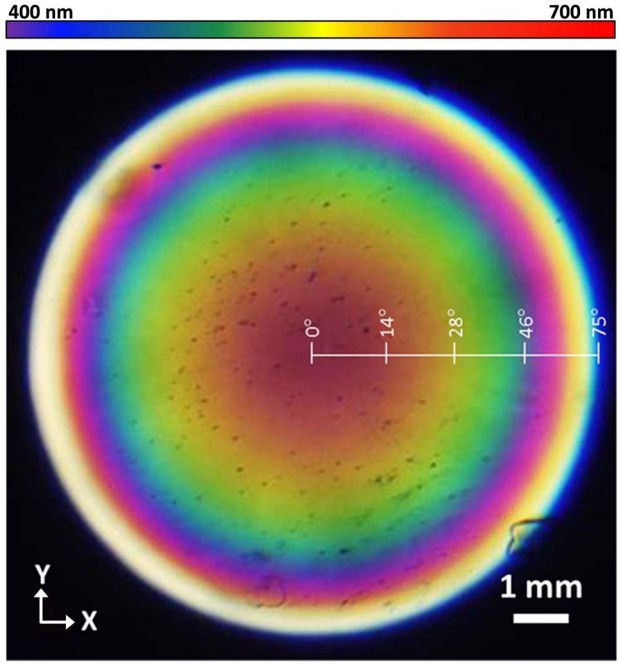

Fig. 3. (Color online) The field distribution of white-light-radial-polarization-induced rainbow rings at the exit pupil of objective lens.

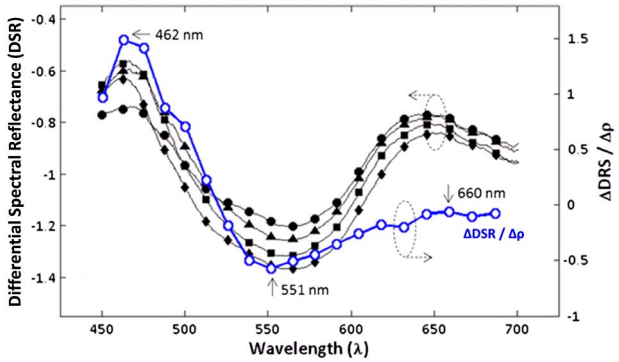

Fig. 4. (Color online) Differential spectral reflectance (DSR) subject to different concentration of NaCl solution, $\rho = 10\%$, 20%, 30%, and 40%, respectively, where the reflectance was subtracted by the baseline of pure water. As we differenced the variation of spectral reflectance with respect to concentration change ($\rho = 10\%$ to 20%), $\Delta\mathrm{DSR}/\Delta\rho$, three peaked wavelengths (462, 551, and 660 nm) were highlighted to feature the most sensitive spectral response.

observed over a wide operation range of wavelength ($\lambda = 400$–700 nm) and angular domain ($\theta = 0$–75 deg).

Up to this point, a system simultaneously capturing the two-dimensional angular/spectral SPR was implemented. We took advantage of highly optical throughput to further pursue a dynamic operation. Equipped with a real-time spectral acquisition system (Chung-Yu Co., USB-100), a proof-of-concept scenario was demonstrated by changing the concentration of a NaCl solution. The variation in concentration caused a dispersive refractive index change, resulting in fine variations on the color appearance of rainbow rings. The information can be extracted and quantified by integrating the intensity of individual color bands via a spectrometer. The normalized differential spectral reflectance (DSR) shown in Fig. 4 presents the variation of spectral reflectance subject to different concentration of NaCl solution, $\rho = 10\%$, 20%, 30%, and 40%, where the reflectance was subtracted by the baseline of pure water. As we differenced the variation of spectral reflectance with respect to concentration change ($\rho = 10\%$ to 20%), $\Delta\mathrm{DSR}/\Delta\rho$, three peaked wavelengths (462, 551, and 660 nm) were found to feature the most sensitive spectral response. The differential signals can be treated as the observation windows for monitoring the concentration change of a salt solution in real time. We expect the proposed scenario to be a useful reference for researchers to highlight or differentiate some unknown biochemical features, a process that currently suffers from inefficiency and time-consuming transitional spectroscopy.

In summary, we have demonstrated a unique far-field feature of plasmonic rainbow rings resulting from a WRP-enabling WRP-SPR sensor integrated with a broadband radial polarizer and a $Au/SiO_2/Au$ sandwich SPR coupler. Based on the collinear setup, the virtual spectral probe mapped a wide spectral/angular range of SPR excitation on the colorful ring pattern at the pupil plane. Combined with a high-speed snapshot spectrum acquisition system, we developed a proof-of-concept scenario where the NaCl liquid concentration change can be monitored in real time. The technique still leaves many opportunities open, and clearly more research must be carried out to explore its full potential. The sensitivity could be further enhanced by coating gold nanoparticles on the top of the metal surface. Also, it can integrated with a super continuum laser source to exploit surface-enhanced Raman scattering for more applications. The preliminary results presented here, however, indicate that the proposed concept could create a major breakthrough in the field of SPR sensors, as it has the potential to move the SPR sensor into rapid, full-spectral practice for monitoring the physical properties of biomacromolecules and protein-protein interactions.

This work was financially supported by the National Science Council (NSC 99-2221-E-009-067-MY3), the Frontier Photonics Research Center/University System of Taiwan, and AU Optronics Corporation.

References

1. W. L. Barnes, A. Dereux, and T. W. Ebbesen, Nature **424**, 824 (2003).
2. J. Homola, Chem. Rev. **108**, 462 (2008).
3. E. Kretschmann and H. Raether, Z. Phys. A **23**, 2135 (1968).
4. A. Otto, Z. Phys. A **216**, 398 (1968).
5. H. Kano and W. Knoll, Opt. Commun. **153**, 235 (1998).
6. Q. W. Zhan, Opt. Lett. **31**, 1726 (2006).
7. K. J. Moh, X. C. Yuan, J. Bu, S. W. Zhu, and B. Z. Gao, Opt. Express **16**, 20734 (2008).
8. R. Vander and S. G. Lipson, Opt. Lett. **34**, 37 (2009).
9. G. Machavariani, Y. Lumer, I. Moshe, A. Meir, and S. Jacket, Opt. Lett. **32**, 1468 (2007).
10. N. Passilly, R. de Saint Denis, K. Ait-Ameur, F. Treussart, R. Hierle, and J. F. O. Roch, J. Opt. Soc. Am. A **22**, 984 (2005).
11. A. Shoham, R. Vander, and S. G. Lipson, Opt. Lett. **31**, 3405 (2006).
12. T. Grosjean, M. Suarez, and A. Sabac, Appl. Phys. Lett. **93**, 231106 (2008).
13. T. H. Lan and C. H. Tien, Opt. Express **18**, 23314 (2010).
14. T. H. Lan, C. Y. Ho, and C. H. Tien, Appl. Phys. Lett. **98**, 081107 (2011).
15. K. J. Moh, X. C. Yuan, J. Bu, S. W. Zhu, and B. Z. Gao, Opt. Lett. **34**, 971 (2009).
16. T. H. Lan, Y. K. Chung, and C. H. Tien, Jpn. J. Appl. Phys. **50**, 09MG04 (2011).